# Simultaneous Recognition of Hand Gestures, Grasping Force, and Hand Aperture Using a Wearable Displacement Myography System

Enrica Stefanelli, Alireza Mohammadi, Chu Wang, Tianshi Yu, Ying Tan, *Fellow, IEEE*, Peter Choong, Francesca Cordella, *Senior Member, IEEE*, Loredana Zollo, *Senior Member, IEEE*, and Denny Oetomo, *Senior Member, IEEE*

***Abstract*—Monitoring forearm muscle activity is essential for estimating human intention in different applications, such as virtual reality (VR), rehabilitation, and prosthetics. While prior studies have mainly focused on recognizing gestures or simultaneously classifying gestures and force, predominantly using surface electromyography (sEMG), the simultaneous classification of gesture, force, and hand aperture within the same gesture has not yet been investigated. This work extends previous approaches by evaluating a wearable displacement myography (DMG)-based system for the combined recognition of hand gestures, four grasping force levels, and multiple hand aperture levels, and by directly benchmarking it against an sEMG system under identical experimental conditions. Data from 13 healthy participants were collected using the MyoLog armband with DMG sensors and sEMG sensors while performing three grasp types (pinch, key, and power) with objects of varying size and four force levels, generating 33 configurations. Across several classifiers, the DMG system achieved a peak accuracy of 93% ± 2%, significantly outperforming EMG (64% ± 10%). DMG showed superior discrimination of hand aperture levels (98% ± 3%), while EMG showed relatively better but still lower performance in force-level classification (82% ± 11%). The results are supported by separability analysis using the Fisher discriminant ratio, which demonstrated consistently higher class separability for DMG. These findings highlight the suitability of DMG for applications requiring precise recognition of hand aperture and force levels, offering a compact, computationally efficient, and stimulation-compatible solution that overcomes several limitations of EMG-based systems.**

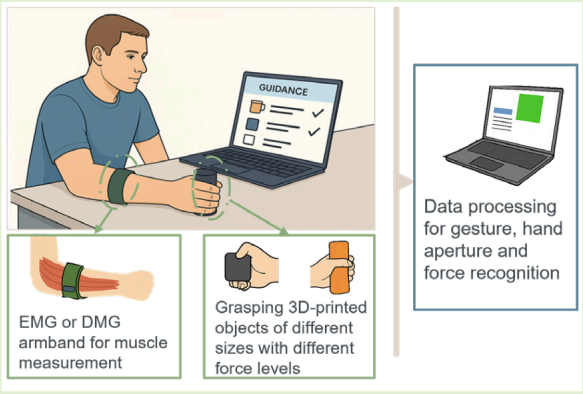


***Index Terms*— Displacement myography (DMG), human–robot interaction, simultaneous gesture–force–aperture classification.**

Received 6 March 2026; accepted 25 March 2026. Date of publication 6 April 2026; date of current version 14 May 2026. This work was supported by the Valma Angliss Foundation. The associate editor coordinating the review of this article and approving it for publication was Prof. Aida Ebrahimi. *(Corresponding author: Enrica Stefanelli.)*

Enrica Stefanelli, Francesca Cordella, and Loredana Zollo are with the Department of Engineering, Research Unit of Advanced Robotics, Human-Centred Technologies, Universitá Campus Bio-Medico di Roma, 00128 Rome, Italy (e-mail: e.stefanelli@unicampus.it; f.cordella@unicampus.it; l.zollo@unicampus.it).

Alireza Mohammadi, Chu Wang, Ying Tan, and Denny Oetomo are with the Department of Mechanical Engineering, The University of Melbourne, Melbourne, VIC 3010, Australia (e-mail: alireza.mohammadi@unimelb.edu.au; Wang.59@unimelb.edu.au; yingt@unimelb.edu.au; doetomo@unimelb.edu.au).

Tianshi Yu is with the Department of Infrastructure Engineering, The University of Melbourne, Melbourne, VIC 3010, Australia (e-mail: tianshi.yu@unimelb.edu.au).

Peter Choong is with the Department of Surgery, Melbourne Medical School, The University of Melbourne, Melbourne, VIC 3010, Australia, and also with St. Vincent's Hospital Melbourne, Melbourne, VIC 3065, Australia (e-mail: pchoong@unimelb.edu.au).

Digital Object Identifier 10.1109/JSEN.2026.3679042

## I. Introduction

MONITORING hand movementsand their interaction with objects is essential across a wide range of applications, including rehabilitation, upper-limb prosthetics, and human–machine interfaces, such as virtual reality (VR) and gaming [1], [2], [3], [4], [5], [6]. These applications relied on accurately detecting hand gestures and postures to enable intuitive interactions or assess functional recovery. Accurate detection of hand gestures, grasping force, and hand aperture, i.e., the degree of hand opening or closing, is critical for enabling intuitive interactions, assessing functional recovery, and providing accurate control in assistive devices. For example, in a VR training simulation, users must manipulate objects of different shapes and sizes naturally, which requires accurate control of both force and hand opening. In rehabilitation, grip strength and hand aperture serve as key indicators of hand function recovery, correlating with functional performance

and patient satisfaction [7], [8]. In prosthetic control, force estimation prevents unintended slippage or excessive pressure, while accurate hand aperture adjustment allows users to grasp objects of different sizes, improving perception of muscle contraction and fine motor control at the residual limb [9].

Traditional methods for tracking hand movements, such as glove-based systems [10] and camera-based tracking [11], face practical limitations including restricted portability, occlusion issues, and discomfort during prolonged use. Glove-based devices can interfere with natural hand movements, while vision-based tracking systems are sensitive to lighting, camera placement, and occlusion, limiting their applicability in real-world settings. As a result, forearm-based sensing approaches that capture muscle activity have emerged as practical and unobtrusive alternatives [12].

Surface electromyography (sEMG) is the most commonly used forearm-based technique, detecting electrical signals generated by muscle contractions to recognize hand gestures and, in some cases, grasping force [12], [13], [14], [15], [16], [17]. High-density sEMG (HD-sEMG) improves spatial resolution and signal quality, enabling higher accuracy for gesture recognition and simultaneous gesture–force estimation. Studies have reported classification accuracies exceeding 90% for common hand gestures, and some have demonstrated reliable simultaneous gesture–force recognition [16]. Despite these advantages, sEMG and HD-sEMG are sensitive to sweat, motion artifacts, fatigue-induced signal degradation, and electrical interference, and often require complex signal processing pipelines [18], [19], [20]. These challenges reduce the reliability of real-time prosthetic and rehabilitation systems, especially during prolonged or dynamic use.

Alternative forearm-based sensing modalities, such as force myography (FMG) and mechanomyography (MMG), have been explored to address some of these limitations [21], [22], [23], [24]. FMG measures volumetric changes, pressure variations, or alterations in light scattering caused by underlying muscle contractions, while MMG captures mechanical vibrations generated by muscle fibers using accelerometers or microphones. These approaches provide noninvasive ways to monitor muscle activity, and studies have demonstrated promising accuracies for gesture recognition and prosthetic control. For example, FMG has been used to control robotic hand orthoses with over 90% classification accuracy across nine hand and wrist gestures [21], while MMG-based systems have achieved up to 98% accuracy using wrist-based pneumatic MMG armbands for not-disabled participants [24]. Despite these successes, FMG and MMG systems still face challenges in simultaneously detecting gesture type, graded force, and hand aperture, limiting their utility in accurate hand control applications.

Displacement myography (DMG) has recently emerged as a promising alternative due to its simple structure, robustness to skin conditions, and compatibility with electrical stimulation [25], [26], [27]. DMG captures subtle mechanical deformations in forearm muscles during activation, offering a unique perspective on muscle function. Previous DMG studies, including our previous work [27], have demonstrated high accuracy for gesture recognition, with wearable armband systems achieving 92%–96% accuracy across multiple gestures. Notably, DMG systems achieved comparable performance to HD-sEMG while employing low-resource machine learning models, minimal signal conditioning, and improved wearability in terms of compactness and ease of placement. Moreover, graded force discrimination and hand aperture classification have not been previously explored using DMG nor have direct, modality-matched comparisons with sEMG been reported for these tasks. Addressing these gaps constitutes a central focus of this study.

While previous research has largely focused on either gesture recognition or simultaneous gesture–force estimation, the combined recognition of gesture type, hand aperture, and graded grasping force within the same grasp remains unexplored. Simultaneous classification of these three factors is critical for applications requiring accurate hand control, such as prosthetic manipulation, rehabilitation assessment, and immersive VR interactions. For example, in rehabilitation, both grip strength and hand aperture serve as functional indicators, and improvements in these metrics correlate with better outcomes. In prosthetics, accurate recognition of all three factors enables more intuitive device control, while, in VR, it allows more natural and immersive interaction with virtual objects.

To address this gap, we present the first evaluation of a DMG-based wearable system capable of simultaneously classifying hand gesture, hand aperture, and graded grasping force. Data were collected from 13 healthy participants using a MyoLog armband equipped with DMG and sEMG sensors, performing three representative grasp types (pinch, key, and power), four force levels, and multiple object sizes, yielding 33 combinations. To evaluate classification performance, we employed four widely used machine learning classifiers [support vector machine (SVM), $K$-nearest neighbors (KNN), linear discriminant analysis (LDA), and random forest (RF)]. The Fisher discriminant ratio analysis was also performed to quantify class separability.

The main contributions of this work are: 1) demonstration of simultaneous recognition of hand gesture, grasping force, and hand aperture using a wearable DMG system and 2) a modality-matched comparison with sEMG, in which both DMG and sEMG sensors are positioned to monitor the same underlying muscle groups in a circular armband configuration, reflecting typical constraints in rehabilitation, prosthesis field, and human–robot interaction applications. This study demonstrates that DMG provides a compact, robust, and stimulation-compatible solution for these scenarios.

## II. Materials and Methods

### A. MyoLog—A DMG-Based Wearable Sensor System

The MyoLog armband [27], shown in Fig. 1(a), is a soft, wearable system consisting of an array of 14 sensor modules embedded in a 3-D-printed flexible thermoplastic polyurethane (TPU) band. The sensor modules are numbered in the Fig. 1(a) from 1 (Ch1) to 7 (Ch7) and from 8 (Ch8) to 14 (Ch14), arranged in ascending order as indicated by the arrows. Each sensor module features a flexible metamaterial structure integrating a neodymium permanent magnet

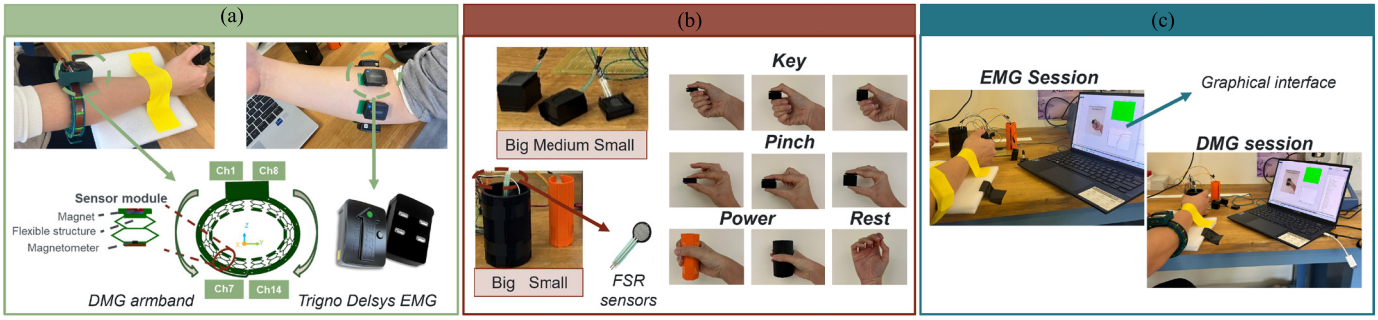


Fig. 1. Experimental setup. (a) DMG armband, comprising a permanent magnet and a magnetometer, was positioned on the forearm as described in [27]. The sensor modules are numbered from 1 (Ch1) to 7 (Ch7) and from 8 (Ch8) to 14 (Ch14), arranged in ascending order as indicated by the arrows. Six Trigno EMG sensors were evenly distributed around the forearm to record muscle activity. (b) Five 3-D-printed objects used in the experiment (three cubes and two cylinders) corresponded to different gestures: key and pinch grasps (three cubes), power grasp (two cylinders), and rest. (c) Experimental protocols for EMG and DMG sessions, together with the graphical interface that provided real-time visual cues to instruct participants on the grasp type and task to execute.

(diameter = 6 mm and thickness = 2 mm) and a triaxis magnetometer (MLX90393, Melexis Inc.). The magnetometers are connected to a microcontroller via a multiplexer (TCA9548A, Adafruit Inc.) on a computational board, which is powered by an 850-mAh lithium-ion battery. Sensor outputs are transmitted to a personal computer via Bluetooth. The sensors measure magnetic field components along three axes ($x$, $y$, and $z$), with the $z$-axis being particularly sensitive to muscle deformations. Variations in the measured magnetic field caused by muscle contractions are used to classify hand gestures, aperture degrees, and grasping forces.

### B. Experimental Setup

The experimental setup is shown in Fig. 1. The EMG sensors and the MyoLog armband [see Fig. 1(a)] were placed over the same forearm muscle groups to ensure that both modalities captured comparable muscle activity patterns, enabling a direct and statistically valid comparison between signals. Both sensor systems were located on the dominant armband of the participants, 4 cm below the elbow, in accordance with the standard placement [28]. In this study, the MyoLog armband was positioned on the forearm as described in [27], ensuring consistent placement across subjects. Each sensor module was mounted such that it was not fully collapsed at rest, allowing approximately 2 mm of displacement during muscle activation and, thereby, maximizing sensitivity to forearm deformations. Regarding the EMG, six Trigno Delsys sensors were equally spaced and arranged in a circular configuration around the subject's forearm of the dominant hand to ensure a comprehensive measurement of both the flexor and extensor muscles.

A MATLAB script (MATLAB R2022b) was developed to record the output of both DMG and EMG modalities. The subjects grasped five objects: three cubes (small: 30 × 25 × 10 mm, medium: 30 × 25 × 20 mm, and big: 30 × 25 × 30 mm) and two cylinders (small: radius = 20 mm and height = 100 mm; big: radius = 40 mm and height = 100 mm), as shown in Fig. 1(b), and printed using polylactic acid or polylactide (PLA). The objects were designed with progressively increasing thickness to induce different degrees of hand aperture. In addition, they were realized also to distribute the force uniformly over the force-sensitive resistors (FSRs) 402 long tail (Interlink Inc.), located inside the objects to measure the grasping force. One FSR sensor was placed inside the cubes, and two were inside the cylinders. A custom board with an Arduino Nano was designed to process and condition the FSR sensors' output signals. Finally, the wrist was stabilized using an elastic tape to ensure consistent positioning across subjects during data acquisition. Although such stabilization does not fully reflect real-time or daily-life conditions, the primary objective of this study was to validate the sensing prototype under controlled and reproducible conditions and to compare the two sensing modalities within the same experimental framework.

### C. Experimental Protocol

The experimental design is shown in Fig. 1(c). The experiments aimed to evaluate the performance of the DMG device in simultaneously discriminating gestures, force levels, and different levels of hand aperture in comparison with the sEMG sensor system. The subjects performed three types of grasps (power, key, and pinch), in addition to a rest position, as shown in Fig. 1(b). The two cylindrical objects were used for the power grasp, while the three cubic objects [see Fig. 1(c)] were employed for the pinch and key grasps. As described in Section II-B, the objects were specifically designed to enable different levels of hand aperture: two for the power grasp (two cylinders) and three for the pinch and key grasps (three cubes).

The experiments are carried out in two sessions, one using DMG and the other using EMG, with seven subjects starting with EMG and six with DMG. Between the two sessions, a time of at least 1 h was considered to avoid muscular fatigue.

In the first part of each session, subjects were initially asked to clean the skin surface with alcohol and then guided by the experimenter and a graphical interface to perform the eight grasping gestures shown in Fig. 1(b) at their maximum force (MF). The subjects had to hold the five objects for 3 s and repeat it three times. The MF based on maximum voluntary contraction (MVC) exerted by each subject was recorded and used to determine the force levels for the next phase.

In the second part of each session, participants performed power, pinch, and key grasps on each object at four force

levels, i.e., 0%, 25%, 50%, and 75% of their MF, as well as a rest condition. MF was defined as the average of three MVCs recorded during the calibration phase. All force targets (25%, 50%, and 75% MF) were computed relative to this subject-specific baseline. This resulted in a total of 33 gesture classes (eight grasping gestures, as shown in Fig. 1(b), performed at four force levels, plus rest). A graphical interface, shown in Fig. 1(c), guided them through the task using a colored bar, where red indicated rest, yellow signaled preparation to grasp, and green indicated the phase where they had to maintain a constant grip within ±10% of the target force for 3 s. Each grasp was repeated three times, with fixed time intervals of 5 s for rest, 7 s for preparation, and 3 s for grasp execution. To prevent fatigue, a 10-s rest was introduced between different force levels and grasps. The order of force levels and grasps was randomized to avoid systematic bias.

### D. Participants

Thirteen subjects (ten males and three females; 12 right-handed and one left-handed) without physical impairment were recruited for this study. All procedures and experiments were approved by The University of Melbourne, Human Research Ethics Committee, project ID 26442. Volunteers were informed about the study, provided with a participant information form, given the opportunity to ask questions, and asked to sign a consent form.

### E. Data Collection

DMG and EMG signals were continuously recorded throughout each trial to capture muscle deformation and electrical activity during hand gestures. EMG data were acquired using the Delsys Trigno system, operating in the standard backward-compatibility mode with a native sampling frequency of 1111.11 Hz (commonly reported as ∼1111 Hz). This corresponds to the manufacturer's internal acquisition rate used for compatibility with legacy Delsys hardware and software configurations. DMG signals were sampled at 10 Hz, which provides sufficient temporal resolution to capture slow muscle displacement dynamics without redundant data, in accordance with the literature [29], [30], [31], [32]. Unlike EMG, which contains high-frequency electrical activity, DMG does not exhibit relevant spectral content above 5–8 Hz. Each trial lasted 15 s and consisted of both grasping and rest phases, during which force measurements were simultaneously logged in real time to track grasp levels.

Force data were collected using FSR sensors connected to an Arduino Nano, which sampled analog readings at ∼ 10 Hz. All data streams were time-synchronized using timestamp-based alignment, ensuring precise temporal matching between EMG, DMG, and FSR signals. This synchronization protocol enabled consistent cross-modal comparisons and minimized potential temporal mismatches that could otherwise affect classification.

### F. Data Processing and Analysis

Once the signals were reordered and synchronized across modalities, only the EMG signals underwent conventional postprocessing, whereas DMG signals were used directly, given their inherent stability and low noise levels, as already demonstrated in [27].

For EMG post-processing, the raw signals were first notch-filtered at 50 Hz to remove power-line interference and then bandpass filtered using a fourth-order Butterworth filter with cutoff frequencies of 10–450 Hz, applied at a sampling frequency of 1111 Hz. The signals were subsequently full-wave rectified, and their envelopes were computed using a 150-ms window with 50-ms overlap. From each segment, five standard time-domain features were extracted: mean absolute value (MAV), slope sign changes (SSCs), waveform length (WL), root mean square (rms), and variance (VAR) [15]. This process yielded a 30-D feature vector per window (five features for each of the six EMG sensors). Finally, EMG features were $z$-score normalized across trials for each subject to reduce intersubject variability. These steps follow best practices in EMG pattern recognition.

In contrast, DMG signals were used directly without filtering. DMG captures slow, large-scale tissue deformation through magnetic field displacement, resulting in inherently low-noise, low-frequency signals (<10 Hz). Prior studies [27] demonstrated that DMG does not benefit from high-pass filtering or feature engineering and is robust to motion artifacts. For the DMG signals, each timestamped sample acquired at 10 Hz (100 ms) was treated as a single input vector to the classifier, corresponding to the instantaneous muscle deformation pattern across sensors. The input dimensionality for DMG was 42 (14 sensors × 3 magnetic field components). As the recording sessions were synchronized via timestamps, DMG samples were temporally aligned to the corresponding force and EMG values.

### G. Separability Analysis

A class separability analysis was performed to evaluate how a group of data was separated from another one and, thus, how it is possible to discriminate muscular activation clusters in two conditions: 1) degree of hand aperture and 2) force levels. Such an analysis is important prior to classification because it provides an understanding of whether the data contain enough discriminative information to separate the classes of interest, to ensure that the classification problem is feasible from a physiological and computational perspective.

In order to achieve this objective, two variances were evaluated by the interclass scatter matrix ($S_b$), which measures the distance between different classes, and the intraclass scatter matrix ($S_w$), which calculates the spread of samples within the same class [33], as

$$S_b = \sum_{j=1}^{c} n_j (m_j - m)(m_j - m)^T$$
$$S_w = \sum_{j=1}^{c} \sum_{k=1}^{n_j} (x_{j,k} - m_j)(x_{j,k} - m_j)^T \quad (1)$$

where $c$ is the number of classes, $x_{j,k} (j = 1, \ldots, c, k = 1, \ldots, n_j)$ represents the $k$th sample of the $j$th class (i.e., one observation of EMG or DMG corresponding to a specific

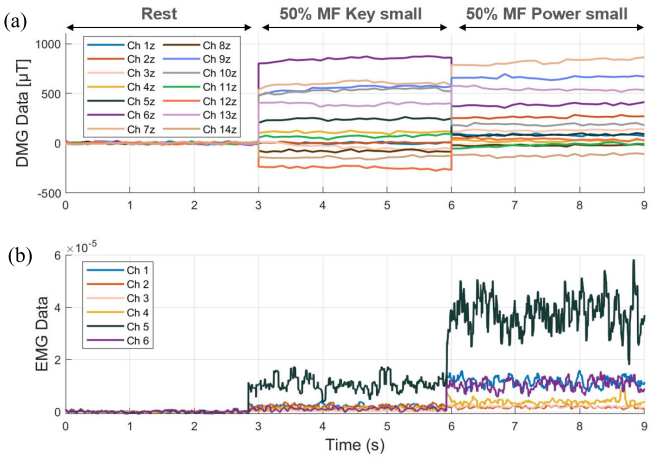


Fig. 2. Representative example of the DMG and EMG trend. The 14 $z$-direction magnetic field signals of the magnetic sensors located in (a) DMG armband and (b) six EMG sensors data during the execution of three hand gestures: rest, key small at 50% MF, and power small at 50% MF.

condition), $m_j$ is the mean vector of the $j$th class (the "center" of all samples belonging to that class), $m$ represents the overall mean calculated from all samples, and $n_j$ is the number of samples in the $j$th class. The ratio between the two matrices, named the Fisher discriminant ratio (FDR) [34], [35], was then obtained. If the FDR value was much greater than 1, the classes were well-separated; if the FDR was equal to 1, there was a moderate level of separability between the classes; if the value was equal to 0, the classes were not separated.

### H. Classification Algorithms and Performance Measures

Four widely recognized machine learning classifiers [27] were employed, i.e., SVM, KNN, LDA, and RF. Considering both EMG features and DMG data, a leave-one-trial-out cross-validation approach was applied to evaluate the performance of the classification models. For each iteration of the cross-validation process, for each subject, one trial was excluded from the training set and used as a test set to assess model performance [36]. By adopting this validation strategy, each trial in the dataset was considered an independent and previously unseen instance during model evaluation and ensures that no identical temporal segment from a given trial appeared in both training and testing. This approach ensures that the classifier's performance reflects its true generalization capability, mimicking real-world operation where new data differ from those encountered during training. It provides a more reliable assessment of how the model would perform in online or real-time applications, where incoming signals are unknown a priori.

Three metrics, i.e., accuracy, precision, and recall, extracted and averaged over the 33 combinations, presented in Section II-C, were calculated. They are labeled as a combination of two letters and a number: the two letters indicate the type of grasp [key (K), pinch (P), and power (Po)] and the object dimensions [small (S), medium (M), and big (B)], while the number indicates the force percentage (0%, 25%, 50%, and 75%). Since the dataset is balanced across classes, the three metrics already provide a comprehensive evaluation of the model's performance. In this context, the $F1$ score, which combines precision and recall, would offer redundant information and was, therefore, not included in the analysis. The classification of 33 combinations encompasses all combinations of hand aperture degrees and force levels, thereby covering the range of real-world activities. In addition, it is paramount to stress the two modalities under high-demand conditions and provide evidence of the classification robustness.

To mitigate potential bias related to the different number of sensors between EMGs and the Myolog armband, an additional analysis was conducted to classify the 33 gesture combinations by using only six sensor modules. These ones were identified in a previous study [27], based on the signal-to-noise ratio (SNR) computed during an MVC task. The results showed that six sensor modules (Ch. 5, 6, 8, 9, 13, and 14, indicated in Fig. 1) exhibited the highest SNR values and were located over the extensor carpi ulnaris (ECU) and flexor carpi ulnaris (FCU) muscles, in accordance with the literature [28], [37].

An additional analysis was carried out to evaluate how well the DMG and EMG sensor systems can distinguish between different force levels when the hand aperture level is kept constant and, conversely, how well they can recognize different hand aperture levels when the force level is fixed. Only the classifiers that achieved the best performance in the initial gesture recognition analysis (involving the classification of 33 gestures) were considered for this evaluation. The accuracy was then calculated individually for each class.

### I. Statistical Analysis

A statistical analysis was carried out to evaluate the performance of the two sensor modalities (DMG and EMG). A Wilcoxon's nonparametric statistical test was applied to the results, selected based on the nonnormal data distribution confirmed by the Shapiro–Wilk test and the paired nature of the samples. The significance level ($p$-value) was set at 0.05.

## III. Results

This section presents the results of the proposed approach, in particular: 1) an example of the DMG and EMG trends to provide insight into the differences and similarities of the two modalities (see Section III-A); 2) the performance of the DMG and EMG data in classifying the 33 combinations considering all the DMG channels and just six channels (see Section III-B); 3) the outcomes of the separability analysis (see Section III-C); and 4) the results of the ability of both systems to distinguish between different hand aperture degrees and force levels (see Section III-D).

### A. DMG and EMG Signals

Fig. 2 illustrates an example of the EMG and DMG signals for three tasks (rest, key small 50% MF and power small 50% MF) of subject 2. The 14 magnets of the DMG device provided three components of the magnetic field ($x$, $y$, and $z$); however, only the $z$-component is displayed since it is the most sensitive to muscle deformation. Considering the EMG,

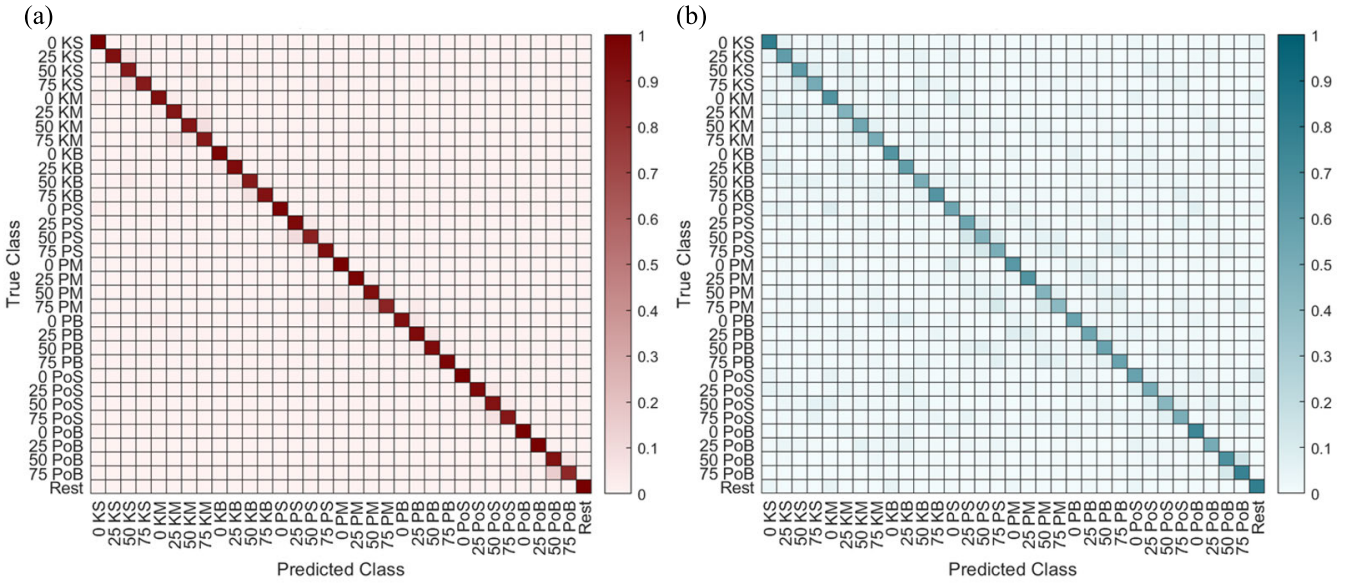


Fig. 3. Classification results of 33 configurations. Confusion matrices of the classifiers that returned the best results for the two modalities. (a) LDA for DMG and (b) RF for EMG. Each class label represents a combination of two letters and a number: $K$ = Key, $P$ = Pinch, and $Po$ = Power; $S$ = Small, $M$ = Medium, and $B$ = big; and numbers indicate the force percentage ($0$ = 0%, $25$ = 25%, $50$ = 50%, and $75$ = 75%).

the filtered signals of all six sensors were reported, whereas the DMG signals are displayed in their raw form without any processing, as discussed in Section II-F. Both EMG and DMG data were subtracted with respect to the rest class.

The DMG data [see Fig. 2(a)] showed stable and low-amplitude signals during the rest phase, reflecting minimal muscle deformation. In the 50% MF key small, there was a noticeable and consistent variation in the signal amplitude across all channels. In the 50% MF power small task, the signals showed distinct profiles that highlight differences in muscle deformation patterns for the two gestures. Notably, the reduction in amplitude observed in some channels compared to rest can be explained by the deformation-based sensing principle of DMG. The DMG signal is approximately proportional to the local radial displacement of the muscle surface

$$S_{\mathrm{DMG}}(t) \propto \Delta d(t). \tag{2}$$

Assuming approximately constant muscle volume, muscle shortening is typically accompanied by radial expansion, whereas lengthening corresponds to a reduction in cross-sectional area. Because muscle contraction involves complex and spatially nonuniform tissue deformation due to anatomical constraints and multimuscle coordination, some regions may experience relative unloading rather than expansion ($\Delta d(t) < 0$), resulting in a decrease in amplitude.

The EMG signals [see Fig. 2(b)], which captured the electrical activity of the muscles, exhibited a higher level of noise compared to the DMGs, despite the implementation of a filtering process. Such consideration was in line with the literature [22] and the intrinsic nature of the two modalities. During the rest phase, the signals exhibited low-amplitude fluctuations, which were characteristic of baseline noise. During the 50% MF key small task, there was a marked increase in amplitude and variability, especially for channels 5, 1, and 6, located on the flexor muscles of the forearm. Similarly,

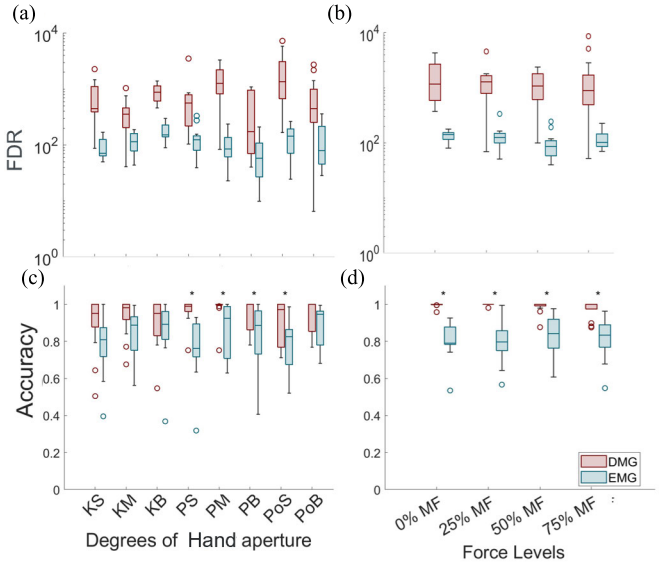


Fig. 4. Results of the FDR and accuracy in discriminating force and degree of hand aperture. Separability analysis results. (a) FDR values for distinguishing between different force levels while keeping the hand aperture levels constant and (b) for distinguishing between different levels of hand aperture while maintaining a constant force level. Accuracy of the LDA classifier (DMG data) and the RF classifier (EMG data) (c) distinguishing between different force levels while keeping the hand aperture level constant and (d) distinguishing between different degrees of hand aperture while maintaining a constant force level. In the $x$-axis, each tick label represents a combination of two letters indicating: $K$ = key, $P$ = pinch, $Po$ = power, $S$ = small, $M$ = medium, and $B$ = big.

the 50% MF power small task showed elevated activity with patterns distinct from the previous phase, reflecting differences in muscle recruitment.

### B. Classification Results of 33 Configurations

The offline analysis, reported in Table I, presents the average and standard deviation of performance metrics (accuracy,

TABLE I
PERFORMANCE PARAMETERS (MEAN ± STANDARD DEVIATION) OF FOUR CLASSIFIERS (LDA, KNN, SVM, AND RF) CALCULATED FOR EACH OF THE 33 PERFORMED GESTURES

| | LDA | | kNN | | SVM | | RF | |
|---|---|---|---|---|---|---|---|---|
| **Metric** | **DMG** | **EMG** | **DMG** | **EMG** | **DMG** | **EMG** | **DMG** | **EMG** |
| Accuracy | **0.93±0.02** | 0.56±0.10 | 0.89±0.04 | 0.47±0.08 | 0.85±0.04 | 0.63±0.10 | 0.89±0.04 | **0.64±0.10** |
| Precision | **0.94±0.04** | 0.55±0.07 | 0.89±0.06 | 0.46±0.09 | 0.86±0.08 | 0.62±0.08 | 0.90±0.06 | **0.63±0.07** |
| Recall | **0.93±0.05** | 0.55±0.09 | 0.89±0.06 | 0.46±0.09 | 0.85±0.06 | 0.62±0.09 | 0.89±0.06 | **0.64±0.10** |

TABLE II
ACCURACY VALUES (MEAN ± STANDARD DEVIATION) OF EMG AND DMG IN DISCRIMINATING BETWEEN DIFFERENT FORCE LEVELS, REPORTED FOR EACH GESTURE

| **Modality** | **Key small** | **Key medium** | **Key big** | **Pinch small** | **Pinch medium** | **Pinch big** | **Power small** | **Power big** |
|---|---|---|---|---|---|---|---|---|
| **DMG** | 0.90±0.16 | 0.93±0.10 | 0.90±0.13 | 0.97±0.07 | 0.98±0.07 | 0.94±0.08 | 0.90±0.12 | 0.93±0.09 |
| **EMG** | 0.79±0.16 | 0.84±0.17 | 0.85±0.17 | 0.76±0.17 | 0.86±0.14 | 0.82±0.18 | 0.78±0.14 | 0.88±0.11 |

TABLE III
ACCURACY VALUES (MEAN ± STANDARD DEVIATION) OF EMG AND DMG IN DISCRIMINATING BETWEEN DIFFERENT HAND APERTURE DEGREES, REPORTED FOR EACH FORCE LEVEL

| **Modality** | **0%MF** | **25%MF** | **50%MF** | **75%MF** |
|---|---|---|---|---|
| **DMG** | 0.99±0.01 | 0.99±0.05 | 0.98±0.03 | 0.97±0.05 |
| **EMG** | 0.81±0.12 | 0.80±0.16 | 0.80±0.09 | 0.80±0.09 |

precision, and recall) for four classifiers (LDA, RF, SVM, and kNN) in discriminating among 33 gestures. A statistical comparison between the EMG and DMG modalities was conducted for each classifier, revealing a statistically significant difference across all performance ($p$-value $= 5.39 \times 10^{-7}$). In addition, the confusion matrices for the classifier that returned the best results in the two modalities (LDA for DMG and RF for EMG) are shown in Fig. 3.

Finally, an analysis was conducted to verify whether the superior number of DMG channels used in the classification could have influenced the results. When considering only six sensor modules, the classification accuracies were LDA: $0.92 \pm 0.04$, kNN: $0.91 \pm 0.001$, RF: $0.91 \pm 0.003$, and SVM: $0.90 \pm 0.003$. Since these results were only slightly lower than those obtained using all sensor modules, the analysis was ultimately performed using the complete set to validate the overall performance and robustness of the MyoLog device as a whole, in line with the objective of this study.

### C. Separability Analysis

A class separability analysis was conducted to assess how well different classes were separated in a dataset. In particular, the FDR was calculated and is shown in Fig. 4. The FDR value for both EMG and DMG in discriminating between the force levels by keeping the hand aperture degrees fixed and the different degrees of hand opening while maintaining the force level constant are reported in Fig. 4(a) and (b), respectively. The results were extracted for each subject on a logarithmic scale. The DMG returned a mean value of the order of $10^3$ for both graphs ($956.6 \pm 1.10 \times 10^3$ and $1.52 \times 10^3 \pm 1.54 \times 10^3$), in line with the results obtained in [27], while, for the EMG, the mean value was approximately in the order of $10^2$ ($121.58 \pm 76.75$, $122.74 \pm 54.20$).

In addition, to provide a visual representation of class separability, a scatter plot of a representative subject was included in which the high-dimensional feature space for EMG and data space for DMG was projected into a 2-D manifold using t-distributed stochastic neighbor embedding (t-SNE). This visualization was generated separately for force level discrimination (Fig. 5(a) for EMG and 5(c) for DMG) and aperture degree discrimination (Fig. 5(b) for EMG and 5(d) for DMG), allowing an intuitive inspection of the clustering structure of the data.

### D. Classification Results of Force Levels and Degree of Hand Aperture

In this section, the capability of the two systems in discriminating between different force levels while maintaining a constant degree of hand aperture and in discriminating between different degrees of hand aperture while maintaining a constant level of force is reported. In particular, the classifiers that returned the best results in the first analysis (LDA for DMG and RF for EMG), shown in Table I, were used to evaluate the performance of the sensors in discriminating force levels [see Fig. 4(c)] and degrees of hand aperture [see Fig. 4(d)]. Regarding force levels discrimination, the mean accuracy value was equal to $0.82 \pm 0.14$ for EMG and $0.94 \pm 0.07$ and DMG. The results showed a statistically significant difference between the EMG and the DMG for pinch small ($p = 0.00048$), pinch medium ($p = 0.0024$), pinch big ($p = 0.039$), and power small ($p = 0.0024$). On the other hand, the mean accuracy was equal to $0.80 \pm 0.12$ for EMG and $0.98 \pm 0.03$ and DMG, with a statistically significant difference at all force levels ($p = 0.00048, 0.00024, 0.00024, 0.00048$). Finally, the mean accuracy value of EMG and DMG was reported for each degree of aperture of the hand (see Table II) and force levels (see Table III).

## IV. DISCUSSION

This study evaluated the performance of the DMG device in discriminating simultaneously gestures, force levels, and different hand aperture levels and compared the results with the EMG.

A first analysis, reported in Table I, was conducted to evaluate the performance of four widely recognized classifiers

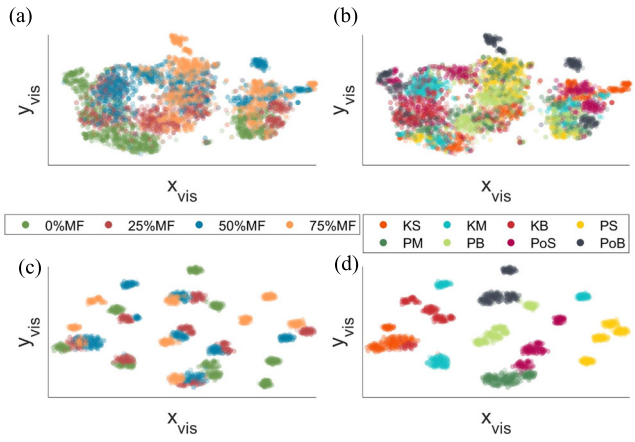


Fig. 5. Visual representation of data separability. t-SNE projection of (a) and (b) EMG feature space and (c) and (d) DMG data illustrating class clustering for (a) and (c) force levels and (b) and (d) finger aperture degrees. (b) and (d) Each label shows a combination of two letters: $K$ = key, $P$ = pinch, $Po$ = power, $S$ = small, $M$ = medium, and $B$ = big.

in discriminating among 33 configurations. It was evident that the DMG outperformed EMG, regardless of the classifier and metric considered. For EMG, RF showed the best performance across all metrics, followed by SVM, while KNN and LDA performed comparably lower. Regarding the DMG, RF slightly outperformed KNN and SVM, while LDA yielded higher results. As demonstrated in Fig. 3, the confusion matrix for the RF for EMG and LDA for DMG revealed that the rest class achieved the highest level of accuracy (0.74 EMG and 0.99 DMG). Regarding DMG, the 0% MF was the easiest to detect compared to the other three force levels of the same gesture, except for pinch big, since 0%, 50%, and 75% MF returned the same accuracy value (0.56). This trend was not replicated by EMG since the results were shown to be strictly dependent on the class performed. However, it was evident that the power gesture of grasping the biggest object (power big) returned the highest value compared to the other groups, regardless of the force level (0.59, 0.48, 0.52, and 0.59 for 0%, 25%, 50%, and 75% MF, respectively). It is worth noting that, although several studies in the literature have reported higher sEMG accuracies for gesture and force recognition tasks, those works typically address gesture or/and force classification, as also reported in Section I. To the best of our knowledge, no previous study has systematically investigated the simultaneous discrimination of gesture, multiple force levels, and hand aperture, as proposed in the present 33-configuration framework. This broader classification setting represents a distinct evaluation scenario compared to conventional paradigms.

To evaluate the robustness of the DMG system, an additional analysis was conducted using only six DMG channels (see Section III-B) instead of the full sensor set. The resulting classification accuracies were comparable to those achieved with all channels, with only a slight decrease when using the full set. This indicates that the DMG system is robust and does not rely on an excessive number of sensors to capture relevant muscle activity. The key channels, located over the flexor and ECU muscles, contained most of the information necessary for gesture discrimination. Nevertheless, the full sensor configuration was maintained in subsequent analyses to maximize performance and fully validate the device's capabilities.

To further investigate the discriminative power of the sensors, the FDR was calculated for both DMG and EMG data [Fig. 4(a) and (b)]. FDR quantifies the separability of classes, with values greater than 1 indicating a higher likelihood of achieving accurate classification. The DMG data consistently showed FDR values above 1 across nearly all gestures, force levels, and hand apertures, reflecting clear differentiation between classes. EMG data also produced FDR values above 1, but with lower averages, indicating relatively less separability. These results demonstrate that DMG captures more distinct patterns of muscle deformation than EMG, particularly for hand aperture, which explains its superior performance in classification tasks.

These observations are consistent with the qualitative distribution of the data shown in the t-SNE projections (see Fig. 5) for a representative subject. In particular, in the MyoLog armband data [see Fig. 5(c)], samples sharing the same force level do not collapse into a single compact cluster; rather, they are organized into multiple well-defined subclusters, each associated with a different finger aperture degree. In Fig. 5(d), when the aperture degree is fixed, four groups corresponding to the different force levels can be identified although they appear more closely spaced and partially overlapping compared to Fig. 5(c). Conversely, the EMG projections [see Fig. 5(a) and (b)] exhibit a less structured clustering pattern, with broader and more overlapping point distributions. This behavior is consistent with the lower FDR values observed for EMG and further supports the higher separability power of DMG data.

Overall, these analyses show that DMG is both robust and highly discriminative. Even with fewer sensors, the system maintains high performance, and its superior class separability supports accurate simultaneous recognition of hand gestures, grasping force, and hand aperture. Together, these findings confirm the suitability of DMG for applications requiring precise upper-limb intention decoding, such as prosthetic control, rehabilitation, and immersive VR interactions.

After evaluating the capability of the dataset to be separable in terms of force and degree of hand aperture discrimination, the accuracy of the classifiers that have returned the best results in the first analysis (LDA for EMG and RF for DMG) was extracted and reported in Fig. 4(c) and (d) and Tables II and III. Considering the discrimination between the force levels, the DMG outperformed EMG across all classes, and the accuracy gap between the sensors seemed more pronounced for pinch small, pinch medium, pinch big, and power small since there is a statistically significant difference between the two modalities. The outperformance of DMG on EMG was also confirmed in hand aperture degrees discrimination for each force level since a statistically significant difference was observed between the two modalities.

A further salient consideration can be extrapolated from the results. In fact, the DMG sensors demonstrated a higher accuracy in discriminating the degrees of hand aperture than the force levels. Different hand aperture degrees probably involved

distinct and localized changes in muscle shape and tissue deformation; consequently, the intrinsic nature of this modality in detecting muscular displacement [22] could effectively capture these spatial patterns. In contrast, EMGs exhibited an inverse trend. Such results could be explained by the fact that smaller motor units were shown to be activated initially, and larger ones were subsequently recruited as the force level increased [38], [39]. This sequence of events resulted in a substantial increase in the amplitude and density of the EMG signal, thereby facilitating the discrimination of varying force levels.

These findings underscore the remarkable capabilities of DMG in monitoring muscle activity, demonstrating its substantial advantages in applications that demand accurate discrimination, such as fine motor control tasks, gestures, and force recognition. Its compact design and ease of integration make it particularly suited for applications requiring mobility and convenience, ensuring accessibility for a wide range of users and environments. In addition, it can be used with electrical stimulation, currently employed to provide sensory feedback to amputees [40], whereas EMG-based approaches may suffer from interference due to their electrical nature. However, EMG confirmed and demonstrated its ability to accurately classify levels of grasping forces, underlining its utility in scenarios involving varying levels of muscle activation, such as dynamic force control in prosthetics.

Despite these encouraging results, some limitations of this study should be acknowledged. First, DMG sensors may be susceptible to magnetic or electromagnetic interference; however, this can be mitigated through appropriate shielding, such as a Faraday cage, to protect the system from external magnetic fields. Second, given the influence of wrist posture and limb position on hand gesture classification reported in previous studies [41], [42], the wrist was stabilized using an elastic tape, and participants were instructed to maintain a constant posture during data acquisition. This choice was made to ensure controlled and reproducible conditions, and is consistent with common practice in offline prosthetics and HRI studies, where subjects are typically required to keep the limb in a fixed position across tasks [43], [44], [45]. While this approach enabled a fair comparison between sensing modalities under standardized conditions, it may limit generalizability to real-world scenarios involving dynamic wrist rotations, limb movements, and trunk compensations. Indeed, several studies have shown that performance degradation can occur when such variations are not incorporated into the training phase [46]. Although including limb position changes during training often results in lower offline accuracy due to increased signal variability, it can significantly improve robustness and generalization in online applications.

## V. Conclusion and Future Works

This work provides the first demonstration of simultaneous classification of hand gesture, grasping force, and hand aperture using a DMG-based wearable system. Across 33 combined classes, DMG consistently outperformed EMG in accuracy, class separability, and robustness, particularly in discriminating aperture levels. Therefore, DMG-based wearable systems could be considered a viable alternative to existing options because of their compact, user-friendly, and wearable design, and compatibility with electrical stimulation.

Future work will focus on testing the device under dynamic conditions, including wrist rotations and limb repositioning, during real-time functional tasks. In this context, it will also be necessary to systematically investigate the optimal sampling frequency for real-time DMG acquisition, as previous studies on FMG [30] have shown that higher sampling rates are required to accurately capture transient muscle deformation and motion-related artifacts during dynamic activities. From a technological perspective, the DMG system will also be explored using a regression-based approach to estimate continuous force levels rather than discrete classes, enabling smoother and more natural real-time control, particularly for prosthetic applications.

## References


[1] S. Geetha, G. Aditya, M. C. Reddy, and G. Nischith, "Human interaction in virtual and mixed reality through hand tracking," in *Proc. IEEE Int. Conf. Electron., Comput. Commun. Technol. (CONECCT)*, Jul. 2024, pp. 1–6.

[2] T. D. Qi, F. L. Cibrian, M. Raswan, T. Kay, H. M. Camarillo-Abad, and Y. Wen, "Toward intuitive 3D interactions in virtual reality: A deep learning- based dual-hand gesture recognition approach," *IEEE Access*, vol. 12, pp. 67438–67452, 2024.

[3] K. Narware, A. Dupalli, A. Ali, P. Dhote, V. Suryawanshi, and P. Falke, "Hand gesture gaming," *Int. J. Multidisciplinary Res.*, vol. 6, no. 2, p. 11, 2024.

[4] Q. Huang et al., "A finger motion monitoring glove for hand rehabilitation training and assessment based on gesture recognition," *IEEE Sensors J.*, vol. 23, no. 12, pp. 13789–13796, Jun. 2023.

[5] J. Xu, P. Mohan, F. Chen, and A. Nürnberger, "A real-time hand motion detection system for unsupervised home training," in *Proc. IEEE Int. Conf. Syst., Man, Cybern. (SMC)*, Oct. 2020, pp. 4224–4229.

[6] D. Blana et al., "Model-based control of individual finger movements for prosthetic hand function," *IEEE Trans. Neural Syst. Rehabil. Eng.*, vol. 28, no. 3, pp. 612–620, Mar. 2020.

[7] R. F. Sampaio, M. C. Mancini, F. C. M. Silva, I. M. Figueiredo, D. V. Vaz, and G. B. De Oliveira Alves, "Work-related hand injuries: Case analyses in a Brazilian rehabilitation service," *Disability Rehabil.*, vol. 28, no. 12, pp. 803–808, Jan. 2006.

[8] H. Yang, J. Wang, and J. Yu, "An analysis of factors affecting hand function after surgery of the injured hand," *Chin. J. Hand Surg.*, vol. 32, pp. 286–288, Apr. 2016.

[9] I. J. R. Martínez, A. Mannini, F. Clemente, and C. Cipriani, "Online grasp force estimation from the transient EMG," *IEEE Trans. Neural Syst. Rehabil. Eng.*, vol. 28, no. 10, pp. 2333–2341, Oct. 2020.

[10] F. Fei et al., "Development of a wearable glove system with multiple sensors for hand kinematics assessment," *Micromachines*, vol. 12, no. 4, p. 362, Mar. 2021.

[11] Y. Liu, M.-Y. Chiu, H. Li, K. Wu, Z. Lei, and Q. Ding, "A real time robust hand tracking method with normal cameras," in *Proc. CCF Chin. Conf. Comput. Vis.*, 2015, pp. 56–65.

[12] L. Zongxing et al., "Human–machine interaction technology for simultaneous gesture recognition and force assessment: A review," *IEEE Sensors J.*, vol. 23, no. 22, pp. 26981–26996, Nov. 2023.

[13] H. Sarwat, A. Alkhashab, X. Song, S. Jiang, J. Jia, and P. B. Shull, "Post-stroke hand gesture recognition via one-shot transfer learning using prototypical networks," *J. NeuroEng. Rehabil.*, vol. 21, no. 1, p. 100, Jun. 2024.

[14] B. Fang et al., "Simultaneous sEMG recognition of gestures and force levels for interaction with prosthetic hand," *IEEE Trans. Neural Syst. Rehabil. Eng.*, vol. 30, pp. 2426–2436, 2022.

[15] B. Xu et al., "Natural grasping movement recognition and force estimation using electromyography," *Frontiers Neurosci.*, vol. 16, Oct. 2022, Art. no. 1020086.

[16] F. Rahimi, M. A. Badamchizadeh, R. C. Sîmpetru, S. Ghaemi, B. M. Eskofier, and A. Del Vecchio, "Simultaneous control of human hand joint positions and grip force via HD-EMG and deep learning," 2024, *arXiv:2410.23986*.

[17] F. Onay and A. Mert, "Phasor represented EMG feature extraction against varying contraction level of prosthetic control," *Biomed. Signal Process. Control*, vol. 59, May 2020, Art. no. 101881. [Online]. Available: https://www.sciencedirect.com/science/article/pii/S1746809420300379

[18] E. Scheme and K. Englehart, "Electromyogram pattern recognition for control of powered upper-limb prostheses: State of the art and challenges for clinical use," *J. Rehabil. Res. Develop.*, vol. 48, no. 6, p. 643, 2011.

[19] X. Yang, C. Castellini, D. Farina, and H. Liu, "Ultrasound as a neurorobotic interface: A review," *IEEE Trans. Syst., Man, Cybern., Syst.*, vol. 54, no. 6, pp. 3534–3546, Jun. 2024.

[20] B. G. Sgambato et al., "High performance wearable ultrasound as a human-machine interface for wrist and hand kinematic tracking," *IEEE Trans. Biomed. Eng.*, vol. 71, no. 2, pp. 484–493, Feb. 2024.

[21] J. Gantenbein, C. Ahmadizadeh, O. Heeb, O. Lambercy, and C. Menon, "Feasibility of force myography for the direct control of an assistive robotic hand orthosis in non-impaired individuals," *J. NeuroEngineering Rehabil.*, vol. 20, no. 1, p. 101, Aug. 2023.

[22] Z. G. Xiao and C. Menon, "A review of force myography research and development," *Sensors*, vol. 19, no. 20, p. 4557, Oct. 2019.

[23] C. S. M. Castillo, S. Wilson, R. Vaidyanathan, and S. F. Atashzar, "Wearable MMG-plus-one armband: Evaluation of normal force on mechanomyography (MMG) to enhance human-machine interfacing," *IEEE Trans. Neural Syst. Rehabil. Eng.*, vol. 29, pp. 196–205, 2021.

[24] S. An, J. Feng, E. Song, K. Kong, J. Kim, and H. Choi, "High-accuracy hand gesture recognition on the wrist tendon group using pneumatic mechanomyography (pMMG)," *IEEE Trans. Ind. Informat.*, vol. 20, no. 2, pp. 1550–1561, Feb. 2024.

[25] S.-G. Cho, M. Yoshikawa, K. Baba, K. Ogawa, J. Takamatsu, and T. Ogasawara, "Hand motion recognition based on forearm deformation measured with a distance sensor array," in *Proc. 38th Annu. Int. Conf. IEEE Eng. Med. Biol. Soc. (EMBC)*, Aug. 2016, pp. 4955–4958.

[26] S.-G. Cho, M. Yoshikawa, M. Ding, J. Takamatsu, and T. Ogasawara, "Machine-learning-based hand motion recognition system by measuring forearm deformation with a distance sensor array," *Int. J. Intell. Robot. Appl.*, vol. 3, no. 4, pp. 418–429, Dec. 2019.

[27] A. Mohammadi, C. Wang, T. Yu, Y. Tan, P. Choong, and D. Oetomo, "An information-rich and highly wearable soft sensor system based on displacement myography for practical hand gesture interfaces," *IEEE J. Biomed. Health Informat.*, vol. 29, no. 5, pp. 3451–3464, May 2025.

[28] F. Riillo et al., "Optimization of EMG-based hand gesture recognition: Supervised vs. unsupervised data preprocessing on healthy subjects and transradial amputees," *Biomed. Signal Process. Control*, vol. 14, pp. 117–125, Nov. 2014.

[29] M. U. Rehman, K. Shah, I. U. Haq, S. Iqbal, M. A. Ismail, and F. Selimefendigil, "Assessment of low-density force myography armband for classification of upper limb gestures," *Sensors*, vol. 23, no. 5, p. 2716, Mar. 2023.

[30] Z. G. Xiao and C. Menon, "An investigation on the sampling frequency of the upper-limb force myographic signals," *Sensors*, vol. 19, no. 11, p. 2432, May 2019.

[31] C. Ahmadizadeh, L.-K. Merhi, B. Pousett, S. Sangha, and C. Menon, "Toward intuitive prosthetic control: Solving common issues using force myography, surface electromyography, and pattern recognition in a pilot case study," *IEEE Robot. Autom. Mag.*, vol. 24, no. 4, pp. 102–111, Dec. 2017.

[32] Z. G. Xiao and C. Menon, "Towards the development of a wearable feedback system for monitoring the activities of the upper-extremities," *J. NeuroEngineering Rehabil.*, vol. 11, no. 1, p. 2, 2014.

[33] J. Gui, Z. Sun, S. Ji, D. Tao, and T. Tan, "Feature selection based on structured sparsity: A comprehensive study," *IEEE Trans. Neural Netw. Learn. Syst.*, vol. 28, no. 7, pp. 1490–1507, Jul. 2017.

[34] T. Yu, R. Garcia-Rosas, A. Mohammadi, Y. Tan, P. Choong, and D. Oetomo, "Separability of input features and the resulting accuracy in classifying target poses for active transhumeral prosthetic interfaces," in *Proc. 43rd Annu. Int. Conf. IEEE Eng. Med. Biol. Soc. (EMBC)*, Nov. 2021, pp. 4615–4618.

[35] T. Yu, A. Mohammadi, Y. Tan, P. Choong, and D. Oetomo, "Sensor selection with composite features in identifying user-intended poses for human-prosthetic interfaces," *IEEE Trans. Neural Syst. Rehabil. Eng.*, vol. 31, pp. 1732–1742, 2023.

[36] G. James, D. Witten, T. Hastie, R. Tibshirani, and J. Taylor, "Statistical learning," in *An Introduction to Statistical Learning: with Applications in Python*. Cham, Switzerland: Springer, 2023, pp. 15–67, doi: 10.1007/978-3-031-38747-0_2.

[37] M. J. Islam et al., "Optimizing electrode positions on forearm to increase SNR and myoelectric pattern recognition performance," *Eng. Appl. Artif. Intell.*, vol. 122, Jun. 2023, Art. no. 106160.

[38] H. P. Clamann, "Motor unit recruitment and the gradation of muscle force," *Phys. Therapy*, vol. 73, no. 12, pp. 830–843, Dec. 1993.

[39] H. Suzuki, R. Conwit, D. Stashuk, L. M. Santarsiero, and E. Metter, "Relationships between surface-detected EMG signals and motor unit activation," *Med. Sci. Sports Exercise*, vol. 34, no. 9, pp. 1509–1517, Sep. 2002.

[40] A. Scarpelli, A. Demofonti, F. Terracina, A. L. Ciancio, and L. Zollo, "Evoking apparent moving sensation in the hand via transcutaneous electrical nerve stimulation," *Frontiers Neurosci.*, vol. 14, p. 534, Jun. 2020.

[41] L. P. Murciego, M. C. Henrich, E. G. Spaich, and S. Dosen, "Reducing the number of EMG electrodes during online hand gesture classification with changing wrist positions," *J. NeuroEng. Rehabil.*, vol. 19, no. 1, p. 78, Dec. 2022.

[42] A. A. Adewuyi, L. J. Hargrove, and T. A. Kuiken, "Evaluating EMG feature and classifier selection for application to partial-hand prosthesis control," *Frontiers Neurorobotics*, vol. 10, p. 15, Oct. 2016.

[43] F. Leone et al., "Simultaneous sEMG classification of hand/wrist gestures and forces," *Frontiers Neurorobotics*, vol. 13, p. 42, Jun. 2019.

[44] Z. Yin et al., "A wearable multisensor fusion system for neuroprosthetic hand," *IEEE Sensors J.*, vol. 25, no. 8, pp. 12547–12558, Apr. 2025.

[45] Z. Lu, S. Cai, B. Chen, Z. Liu, L. Guo, and L. Yao, "Wearable real-time gesture recognition scheme based on A-mode ultrasound," *IEEE Trans. Neural Syst. Rehabil. Eng.*, vol. 30, pp. 2623–2629, 2022.

[46] S. M. Engdahl, S. A. Acuña, E. L. King, A. Bashatah, and S. Sikdar, "First demonstration of functional task performance using a sonomyographic prosthesis: A case study," *Frontiers Bioeng. Biotechnol.*, vol. 10, May 2022, Art. no. 876836.

**Enrica Stefanelli** received the B.Sc. degree in industrial engineering, the M.Sc. degree in biomedical engineering, and the Ph.D. degree in bioengineering from Universitá Campus Bio-Medico di Roma, Rome, Italy, in 2018, 2021, and 2025, respectively.

She is currently a Postdoctoral Researcher of Bioengineering at the Universitá Campus Bio-Medico di Roma and a member of the Research Unit of Advanced Robotics and Human-Centered Technologies (CREO Lab). Her research focuses on upper-limb prosthetic device control and sensorization, aiming to optimize prosthetic behavior during grasping and manipulation tasks by replicating the human somatosensory systems.

**Alireza Mohammadi** received the B.Sc. degree from Iran University of Science and Technology, Tehran, Iran, in 2005, the M.Sc. degree in mechanical engineering from Sharif University of Technology, Tehran, in 2008, and the Ph.D. degree from The University of Melbourne, Melbourne, VIC, Australia, in 2014.

He is currently a Senior Research Fellow at the Human Robotics Laboratory, The University of Melbourne. His research interests include soft robotics, wearable robotics, and prosthetics.

**Chu Wang** received the B.Eng. degree from China Agricultural University, Beijing, China, in 2020, and the M.Eng. degree in mechanical engineering from The University of Melbourne, Melbourne, VIC, Australia, 2023, where she is currently pursuing the Ph.D. degree with the Department of Mechanical Engineering, Human Robotics Laboratory.

Her research interests include dexterous hand manipulation and prosthetic hand control.

**Tianshi Yu** received the B.Eng. degree from Zhejiang University, Hangzhou, China, in 2017, and the M.Eng. degree in mechatronics engineering and the Ph.D. degree from The University of Melbourne, Melbourne, VIC, Australia, 2019.

He is currently a Research Fellow at the Department of Infrastructure Engineering, The University of Melbourne. His research interests include human–robot interaction, assistive robotics, and prosthetics.

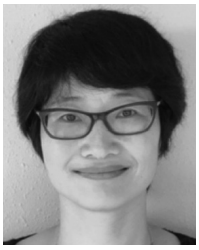

**Ying Tan** (Fellow, IEEE) received the bachelor's degree from Tianjin University, Tianjin, China, in 1995, and the Ph.D. degree from the National University of Singapore, Singapore, in 2002.

Following her doctoral studies, she undertook a Postdoctoral Fellowship at the Department of Chemical Engineering, McMaster University, Hamilton, ON, Canada, in 2002, before joining The University of Melbourne, Melbourne, VIC, Australia, in 2004, where she is a Professor with the Department of Mechanical Engineering. Her exceptional research contributions have earned her prestigious accolades, including Australian Postdoctoral Fellowship from 2006 to 2008 and a Future Fellowship from Australian Research Council (ARC) from 2009 to 2013. Her research interests include diverse spanning intelligent systems, nonlinear systems, data-driven optimization, rehabilitation robotic systems, human motor learning, wearable sensors, and model-guided machine learning.

Dr. Tan serves as a member of the College of Experts (COE) of the ARC from 2024 to 2026. She is widely recognized as a Distinguished Scholar in her field, holding the esteemed titles of a Fellow of the Institution of Engineers of Australia (FIEAUST) and Asia–Pacific Artificial Intelligence Association. She was also a Committee Member from 2024 to 2025.

**Peter Choong** is a Distinguished Melbourne-Based Orthopedic Surgeon, a Medical Leader, and a Researcher, renowned for his expertise in bone/soft tissue tumors and joint replacement, holding key roles at The University of Melbourne, Melbourne, VIC, Australia (a Head of Surgery), and St. Vincent's Hospital (the Sir Hugh Devine Chair), with extensive international training at Mayo Clinic, Stockholm, Sweden, and significant contributions to medical education, innovation (BioFab3D), and advanced orthopedic care, including being honored with an Officer of the Order of Australia.

**Francesca Cordella** (Senior Member, IEEE) received the Laurea degree in electronic engineering and the Ph.D. degree in computer and automation engineering from the University of Naples Federico II, Naples, Italy.

She is currently an Associate Professor of Bioengineering at the University Campus Bio-Medico of Roma, Rome, Italy. Her research interests are mainly in the field of biomechanics, biomedical robotics, bionics, human–machine interfaces, and physical and cognitive human–robot interaction.

Dr. Cordella is the Co-Chair of the IEEE/RAS Technical Committee on Rehabilitation and Assistive Robotics. She was and is involved in the role of the Co-PI and the Project Manager of the scientific responsibility of the Work Package in more than 25 European and national projects in her areas of expertise. She has authored/co-authored three patents and more than 120 peer-reviewed publications that appeared in international journals, books, and conference proceedings.

**Loredana Zollo** (Senior Member, IEEE) is currently a Full Professor of Bioengineering and the Head of the Advanced Robotics and Human-Centre Technologies (CREO Lab), Università Campus Bio-Medico di Roma, Rome, Italy, where she is a Co-Ordinator of the Ph.D. in bioengineering, applied sciences and intelligent systems. She has 238 publications registered on Scopus, with 5309 total citations and an H-index of 35. She is a PI of several national and European projects. Her research interests include rehabilitation and assistive robotics, bio-robotics and bionics, human–machine interfaces, and collaborative robotics.

Dr. Zollo is a member of the editorial board and an associate editor of several journals and conferences.

**Denny Oetomo** (Senior Member, IEEE) received the B.Eng. (Hons.) degree from The Australian National University, Canberra, ACT, Australia, in 1997, and the Ph.D. degree from the National University of Singapore, Singapore, in 2004.

In 2008, he joined the Department of Mechanical Engineering, The University of Melbourne, Melbourne, VIC, Australia, where he is currently a Professor. His research interests include robot dynamics and manipulation and human–robot interaction, with industrial and clinical applications of these capabilities, such as in robot-assisted rehabilitation, assistive robotics, and neuroprosthetics.

Dr. Oetomo served as an Associate Editor for IEEE TRANSACTIONS ON MECHATRONICS and *Robotics and Automation Letters*, among others. He is currently an Associate Editor of IEEE TRANSACTIONS ON NEURAL SYSTEMS AND REHABILITATION ENGINEERING.

Open Access funding provided by 'Universita Campus Bio-Medico di Roma' within the CRUI CARE Agreement